

Article

A Novel Calculate Model of Shear Deformation and Relative Displacement of Pile–Soil Interface in Warm Frozen Soil Foundation

Gaochen Sun ^{1,*} , Lijun Gu ², Long Li ¹, Yufan Huo ¹, Zhengzhong Wang ³  and Hongzu Dang ²

¹ School of Civil Engineering, Xi'an Shiyou University, Xi'an 710065, China; 17730623101@163.com (L.L.); 13379589757@163.com (Y.H.)

² China State Construction Engineering Corporation Aecom Consultant Co., Ltd., Lanzhou 730000, China; sdkjdxglj@163.com (L.G.); danghongzu212@163.com (H.D.)

³ College of Water Resources and Architectural Engineering, Northwest A&F University, Yanglin 712100, China; wangzz0910@163.com

* Correspondence: maomaosgc@163.com

Abstract: In permafrost regions with warm frozen soil, the pile foundation is commonly used, but most currently available models for the WFS foundation pile–soil system are either highly empirical or overcomplicated, without a simplified theoretical manner in engineering. This study derives a novel and simplified calculated model of the WFS pile–soil system. The model is formulated in terms of the shear deformation theory and load transfer method based on the rigorous deformation mechanism of the WFS foundation soil around the pile. Considering the different depth soil features and the equilibrium state of the pile–soil system, dividing warm frozen soil foundation into three regions (TPPR, ER, and BPPR) to calculate the D_p and D_s can simply obtain the total displacement of pile under different loads. The results demonstrate that the present theoretical model can well predict the WFS foundation load–displacement response of the pile. The present model provides a simple, practical, and effective approach for the estimation of the load–displacement behavior of piles installed in the WFS foundation.

Keywords: warm frozen soil; pile foundation; shear displacement method; load transfer theory



Citation: Sun, G.; Gu, L.; Li, L.; Huo, Y.; Wang, Z.; Dang, H. A Novel Calculate Model of Shear Deformation and Relative Displacement of Pile–Soil Interface in Warm Frozen Soil Foundation. *Buildings* **2024**, *14*, 1459. <https://doi.org/10.3390/buildings14051459>

Academic Editor: Eugeniusz Koda

Received: 8 April 2024

Revised: 7 May 2024

Accepted: 14 May 2024

Published: 17 May 2024



Copyright: © 2024 by the authors. Licensee MDPI, Basel, Switzerland. This article is an open access article distributed under the terms and conditions of the Creative Commons Attribution (CC BY) license (<https://creativecommons.org/licenses/by/4.0/>).

1. Introduction

As China attaches great importance to the social and economic development of Tibet, Northeast China, and other regions and steadily advances the strategic measures for the development of the West, the construction of projects in permafrost regions is in full swing. Pile foundation, as a common form of foundation structure for frozen soil foundation in permafrost regions, is widely used for its strong adaptability, stability, and high bearing capacity [1–4]. However, with the aggravation of the global warming trend, the degradation of frozen soil foundations and the generation of large areas of high-temperature and highly warm frozen soil foundations have become the premise of disturbing the healthy development of frozen soil engineering [5,6]. At present day, in some extremely unstable areas in the permafrost region, the corresponding “bridge instead of road” dry bridge is adopted as the foundation of engineering structures [7–10]. However, the interaction between the foundation pile and soil in warm frozen soil foundation and the displacement relationship of the foundation pile under the action of upper load have always been the focus of pile foundation research in warm frozen soil regions, so it is urgent to establish the load–displacement theoretical relationship between pile–WFS system in warm frozen soil foundation.

Many studies have been conducted on the theory and numerical calculation of pile foundations in frozen soil over the years. Semenova N.P [11] proposed a calculation method for the settlement of foundation in thawing frozen soil with a small permeability coefficient

by studying the settlement of structure foundation in thawing frozen soil. Abzhalimo [12] analyzed the interaction mechanisms between frozen soil and an immovable foundation. Zhao XY et al. [13] used two numerical modeling approaches: solid-fluid coupled finite element (FE) modeling and the beam-on-nonlinear-Winkler-foundation (BNWF) method to calculate the pile P - D curves in frozen ground crust overlying liquefiable soils. Li L and Deng YS [14] based on the transparent soil model test technique and Coupled Eulerian–Lagrangian (CEL) approach, single pile penetration tests were conducted. The load-vertical displacement characteristics of composite foundation and the variation of soil around piles are analyzed and compared with circular piles with the same cross-sectional area. Wang HL and Zhang JM et al. [15] using a numerical model considering the interface interaction between frozen soil and SCC was established for interpreting the bearing mechanism of composite foundation. Tang LY et al. [16] proposed a calculation method to predict the bearing capacity of frozen soil pile foundations based on atmospheric temperature change, aiming at the connection between atmospheric temperature change and the bearing capacity of frozen soil pile foundations. It can be seen that although previous studies have analyzed the interaction mechanisms between pile and frozen soil, few studies exist on the theory of the pile-WFS system. So it is urgent to find a load transfer model with low calorific value materials and design parameters obtained through laboratory tests to guide engineering practice.

Through the analysis of the overall deformation mode of foundation piles in warm frozen soil foundation, it can be found that the total settlement displacement of foundation piles in warm frozen soil foundation consists of two parts: the relative displacement D_p of foundation pile-frozen soil interface and the displacement D_s of frozen soil around pile outside the interface, as shown in Figure 1 [17–20], that is, the total displacement of pile body in warm frozen soil foundation can be obtained by calculating these two parts respectively by scientific and reasonable means. However, due to the particularity of the warm frozen soil foundation, the interaction between the foundation pile and the frozen soil around the pile is closely related to the temperature [21–25]. Therefore, this paper divides the warm frozen soil foundation into different temperature regions and, firstly, establishes the characterization of different temperature regions ($-1\text{ }^{\circ}\text{C} \leq T \leq 0\text{ }^{\circ}\text{C}$, warm frozen soil region, $T < -1\text{ }^{\circ}\text{C}$, Permafrost regions). The pile–soil interface load transfer model is based on pile side friction resistance and pile–soil interface relative displacement, and the relative displacement of the pile–soil surface is obtained based on the interface load transfer principle. At the same time, the distribution forms of pile side friction resistance in different regions of warm frozen soil foundation on the pile side are obtained according to the calculation results. Then, according to the shear displacement method and the load transfer principle of frozen soil foundation, the pile–soil relative slip of foundation in different regions under the warm frozen soil foundation and the shear deformation of frozen soil around the pile are comprehensively considered to obtain the pile–soil interface displacement, which more accurately reflects the deformation mechanism of foundation pile in warm frozen soil foundation.

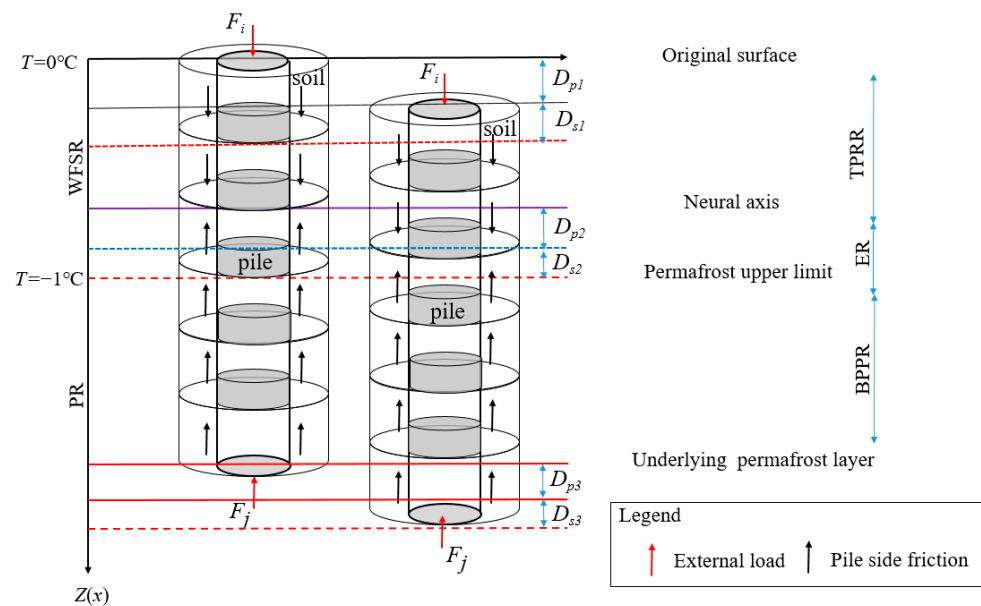


Figure 1. Cement-mixed batter piles composite foundation of the warm frozen soil (WFS) subgrade model prototype.

2. Description of Models

2.1. Assumption

Considering the complexity of the foundation environment of warm frozen soil, a simplified consolidation model is adopted based on the following assumptions:

- (1) Vertical compression deformation of the foundation and frozen soil around the pile is considered, and radial displacement under upper load is not considered; one-dimensional uniform compression deformation occurs in the underlying permafrost soil foundation.
- (2) The soil settlement at the neutral plane of the composite foundation is equal to that at the neutral plane of the pile unit body, and the soil settlement between the piles is equal, and the other positions are different; On any plane, the stress and settlement of piles are the same, and the distribution of stress and settlement of soil between piles is non-uniform.
- (3) The soil around the pile is composed of the soil at the pile–soil interface and the soil outside the pile–soil interface. The soil at the pile–soil interface and the pile body have nonlinear slip, and the thickness of this part of the soil is ignored during calculation; Shear deformation occurs outside the interface of pile and soil.
- (4) The total displacement of the foundation pile in the WFS environment is composed of the displacement D of soil around the pile relative to D_p at the pile–soil interface, and the displacement D_s outside the pile–soil interface are shown in Equation (1):

$$D = D_p + D_s \quad (1)$$

where D_p is calculated by the pile–soil interface load transfer principle, and D_s is calculated by the shear displacement method.

2.2. Establishment of Computational Model

2.2.1. Simplified Friction Resistance of Pile in WFS Foundation

The interaction between pile and soil in warm frozen soil foundation is complicated, and there are essential differences between the interaction between pile and frozen soil in different regions. It is particularly important to select a proper pile–soil function model to express the relationship between pile side friction and settlement of pile and soil for the stress-displacement analysis of piles in warm, frozen soil foundations [26–31]. According

to the position and deformation mechanism of the foundation pile in the frozen soil foundation, the above theoretical hypothesis (3) and the location of the upper limit of frozen soil, the position of the pile foundation in the warm frozen soil foundation can be divided into two pile segments and three regions, as shown in Figure 2:

- (1) (TPPR) Plastic deformation region of pile top ($-1\text{ }^{\circ}\text{C} \leq T \leq 0\text{ }^{\circ}\text{C}$, $0 < z \leq x_1$)

TPPR is located at the top of the pile ($0 < z \leq x_1$), and the pile section is located in the warm frozen soil section. The plastic deformation is mainly manifested in the form of TPPR, and the regional displacement is composed of the pile top displacement D_{p1} and the soil displacement D_{s1} around the pile. When the plastic deformation in this region reaches the maximum, its stress reaches the maximum τ_{u1} .

- (2) (ER) Elastic deformation region in pile ($-1\text{ }^{\circ}\text{C} \leq T \leq 0\text{ }^{\circ}\text{C}$, $x_1 < z \leq x_3$)

ER is located in the middle of the pile ($x_1 < z \leq x_3$), and the pile section is located in the warm frozen soil section. The elastic deformation is mainly manifested in the form of ER, and the regional displacement is composed of the pile top displacement D_{p2} and the soil displacement D_{s2} around the pile. When the plastic deformation in this region reaches the maximum, its stress reaches the maximum τ_{u2} .

- (3) (BPPR) Plastic deformation region of pile bottom ($T < -1\text{ }^{\circ}\text{C}$, $x_3 < z \leq x_4$)

BPPR is located at the bottom of the pile ($x_3 < z \leq x_4$), and the pile section is located in the permafrost soil section. The elastic deformation is mainly manifested in the form of BPPR, and the regional displacement is composed of the pile top displacement D_{p3} and the soil displacement D_{s3} around the pile. When the plastic deformation in this region reaches the maximum, its stress reaches the maximum τ_{uf} .

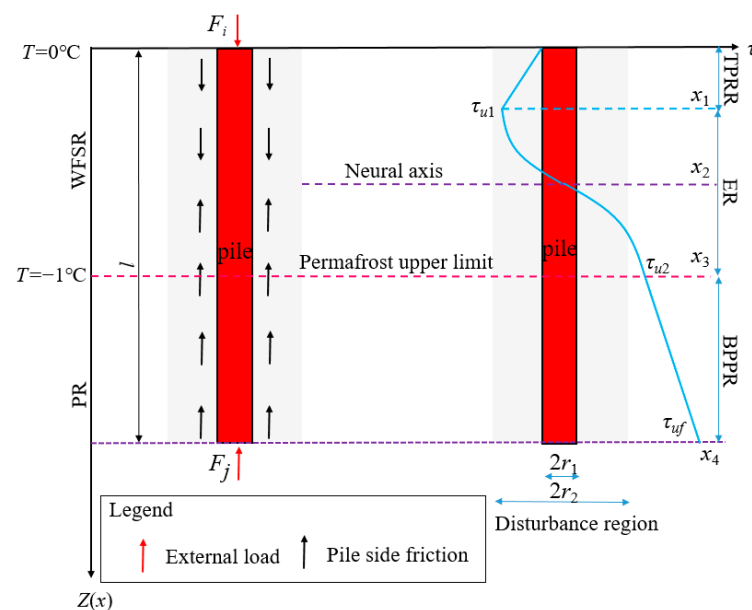


Figure 2. Distribution of lateral frictional resistance of pile foundation for WFS.

Two states of frozen stability and melting correspond to the above division of piles in warm frozen soil, and the stress-strain relation of the pile–soil contact surface is the key to the establishment of this model. Therefore, for piles in the warm, frozen soil foundation region, the ambient temperature is high, and the ice crystals in the soil are in a melting state. Combined with the relation of the pile–soil contact surface on soft soil foundation, The stress-strain constitutive relation model based on the soft soil model is adopted by

referring to the test of the contact surface between frozen silty soil and concrete in frozen Qinghai-Tibet. Specific interactions between regions are shown in Equation (2):

$$\tau(z) = \begin{cases} C + K_0[\gamma z + \sigma(z)] \tan \varphi & x \in [0, x_1] \\ \tau_{u2} \frac{z-\delta}{x_3-\delta} & x \in (x_1, x_3] \\ A \times [1 - B \exp(-C \times \varepsilon)] & x \in (x_3, x_4] \end{cases} \quad (2)$$

where $\tau(z)$ is the different regions shearing stress; C is the WFS Cohesive force, kPa; $\sigma(z)$ is normal stress which existed in TPPR of pile, kPa; φ is the WFS Angle of internal friction, °; δ is the neutral axis position, m; z is the depth from the surface ground, m; τ_{u2} is the biggest shearing stress in ER; A , B , and C are functions of temperature t and water content ω ; τ_{uf} is the biggest shearing stress in BPPR.

2.2.2. WFS Calculate Model Features

The WFS Calculate Model (WFSCM) Features employs shearing theory and load transfer theory to calculate the pile displacement D_p and soil displacement D_s . Compared to the traditional calculation model, The WFSCM has the following features:

- (1) The model parameters are simplified. Compared to the traditional model, the calculated model only requires the soil's physical and mechanical parameters for calculations.
- (2) According to the temperature zone divided by the soil regions, let calculation results is more accurate. (TPPR) Plastic deformation region of pile top ($-1\text{ }^\circ\text{C} \leq T \leq 0\text{ }^\circ\text{C}$, $0 < z \leq x_1$) (ER) Elastic deformation region in pile ($-1\text{ }^\circ\text{C} \leq T \leq 0\text{ }^\circ\text{C}$, $x_1 < z \leq x_3$) (BPPR) Plastic deformation region of pile bottom ($T < -1\text{ }^\circ\text{C}$, $x_3 < z \leq x_4$)
- (3) The method is based on the shearing theory and load transfer theory, modified on the basis of a series of findings from theoretical analysis, experimental research, and engineering practice.

2.3. Establishment of Basic Equation

At present, there are many theories for the calculation and analysis of pile–soil contact, such as the load transfer method, elastic theory method, shear deformation method, and so on [3,32–41]. This paper mainly analyzes the stress distribution of pile foundation in WFS foundation through the load transfer method and shear displacement method. The load transfer method assumes that the pile itself is divided into multiple equal-length elements, and there are elastic deformation coordination conditions among each individual element, and the soil micro-elements in the WFS foundation are analyzed [42–47], as shown in Figure 3.

According to the above conditions, the static equilibrium condition equation of soil between piles in WFS can be expressed as Equations (3)–(8).

- (1) Force balance of pile element, the balance equation was shown in Equation (3)

$$\begin{cases} \sigma_p(z)A_p + \tau(z)U_p dz - [\sigma_p(z) + d\sigma_p]A_p = 0 & x \in [0, x_2] \\ \sigma_p(z)A_p - \tau(z)U_p dz - [\sigma_p(z) + d\sigma_p]A_p = 0 & x \in (x_2, x_4] \end{cases} \quad (3)$$

simplify the Equation (3) was shown in Equation (4)

$$\begin{cases} \sigma_p = \frac{U_p}{A_p} \tau(z) dz = \frac{2}{r_1} \tau(z) dz & x \in [0, x_2] \\ \sigma_p = -\frac{U_p}{A_p} \tau(z) dz = -\frac{2}{r_1} \tau(z) dz & x \in (x_2, x_4] \end{cases} \quad (4)$$

- (2) Force balance of soil element, the balance equation was shown in Equation (5)

$$\begin{cases} \sigma_s(z)A_s + \tau(z)U_s dz - [\sigma_s(z) + d\sigma_s]A_s = 0 & x \in [0, x_2] \\ \sigma_s(z)A_s - \tau(z)U_s dz - [\sigma_s(z) + d\sigma_s]A_s = 0 & x \in (x_2, x_4] \end{cases} \quad (5)$$

simplifying Equation (5) was shown in Equation (6)

$$\begin{cases} d\sigma_s = -\frac{U_s}{A_s}\tau(z)dz & x \in [0, x_2] \\ d\sigma_s = \frac{U_s}{A_s}\tau(z)dz & x \in (x_2, x_4] \end{cases} \quad (6)$$

By substituting Equation (3) into Equations (4) and (6), the differential equation can be solved; the solved equation was shown in Equations (7) and (8)

$$\begin{cases} \sigma_{p1} = \frac{U_p}{A_p} [Cz + K_0[\frac{\gamma z^2}{2} + \sigma(z)z \tan \varphi] + c_1 & x \in [0, x_1] \\ \sigma_{p2} = \frac{U_p}{A_p} [\tau_{u2} \frac{(\frac{z^2}{\delta} - z)}{(\frac{x_3}{\delta} - 1)}] + c_2 & x \in (x_1, x_3] \\ \sigma_{p3} = \frac{U_p}{A_p} \{A \times [1 - \exp(-B \times \varepsilon)]z\} + c_3 & x \in (x_3, x_4] \end{cases} \quad (7)$$

$$\begin{cases} \sigma_{s1} = \frac{U_s}{A_s} [Cz + K_0[\frac{\gamma z^2}{2} + \sigma(z)z \tan \varphi] + c_4 & x \in [0, x_1] \\ \sigma_{s2} = \frac{U_s}{A_s} [\tau_{u2} \frac{(\frac{z^2}{\delta} - z)}{(\frac{x_3}{\delta} - 1)}] + c_5 & x \in (x_1, x_3] \\ \sigma_{s3} = \frac{U_s}{A_s} \{A \times [1 - \exp(-B \times \varepsilon)]z\} + c_6 & x \in (x_3, x_4] \end{cases} \quad (8)$$

where, δ_{p1} , δ_{p2} and δ_{p3} are pile normal stress in different regions, kPa; δ_{s1} , δ_{s2} and δ_{s3} are soil normal stress in different regions, kPa; A_p is the pile area, m²; U_p is the pile perimeter, m; A_s is the soil ring area, m²; U_s is the soil ring perimeter, m; $c_1 \sim c_6$ is the constant for equation.

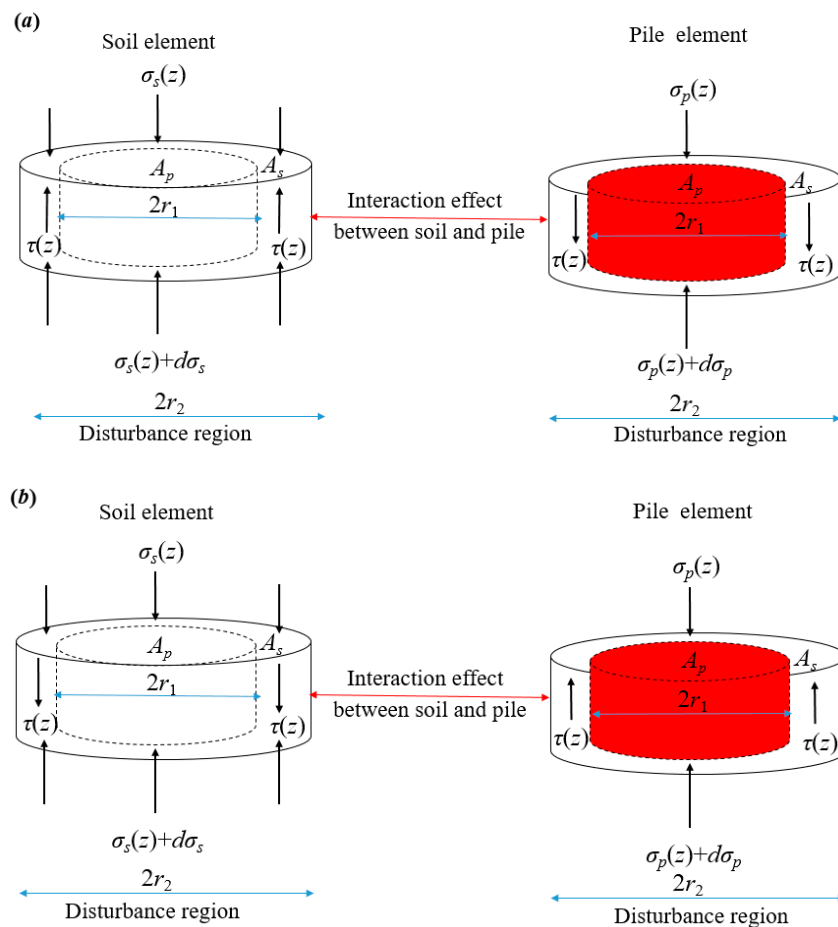


Figure 3. Vertical force diagram for pile and soil elements (a) above the neutral axis; (b) down the neutral axis.

2.4. Load Transfer Analysis of Pile–Soil System of Pile Foundation in WFS

According to the division principle of pile–soil system in Section 2.2.1 description, the WFS pile foundation is divided into the plastic zone at the top of the pile, the elastic zone in the middle of the pile, and the plastic zone at the bottom of the pile. The total displacement of the pile is obtained by solving the displacement of the pile body in each region and the displacement of the soil outside the pile–soil interface.

2.4.1. Pile Displacement Calculation

Taking the pile element as the research object, combined with load transfer theory, vertical compression of the pile element was shown in Equation (9).

$$\begin{aligned} dD_p &= -\frac{F(z)}{A_p E_p} dz \\ &= -\frac{\sigma(z)}{E_p} dz \end{aligned} \quad (9)$$

where E_{p1} is the modulus of elasticity for pile materials, MPa.

(1) Pile displacement calculation for TPPR

By substituting Equation (7) σ_{p1} equation into Equation (9), TPPR displacement D_{p1} can be solved, as shown in Equation (10).

$$\begin{aligned} D_{p1} &= \int_0^{x_1} -\frac{\sigma_{p1}}{E_p} dz \\ &= \int_0^{x_1} -\left\{ \frac{U_p}{A_p E_p} \left[Cz + K_0 \left[\frac{\gamma z^2}{2} + \sigma(z)z \right] \tan \varphi \right] + c_1 \right\} dz \end{aligned} \quad (10)$$

(2) Pile displacement calculation for ER

By substituting Equation (7) σ_{p2} equation into Equation (9), ER displacement D_{p2} can be solved, as shown in Equation (11).

$$\begin{aligned} D_{p2} &= \int_{x_3}^{x_2} -\frac{\sigma_{p2}}{E_p} dz \\ &= \int_{x_3}^{x_2} -\left\{ \frac{U_p}{E_p A_p} \left[\tau_{u2} \frac{\left(\frac{z^2}{\delta^2} - z \right)}{\left(\frac{x_3^2}{\delta^2} - 1 \right)} \right] + c_2 \right\} dz \end{aligned} \quad (11)$$

(3) Pile displacement calculation for BPPR

By substituting Equation (7) σ_{p3} equation into Equation (9), ER displacement D_{p3} can be solved, as shown in Equation (12).

$$\begin{aligned} D_{p3} &= \int_{x_3}^{x_2} -\frac{\sigma_{p3}}{E_p} dz \\ &= \left\{ \int_{x_3}^{x_4} \frac{U_p}{E_p A_p} \left\{ A \times [1 - \exp(-B \times \varepsilon)]z \right\} + c_3 \right\} dz \end{aligned} \quad (12)$$

2.4.2. Soil Displacement Calculation Outside the Pile–Soil Interface

Taking the soil element as the research object, combined with the shear displacement principle, shear stress at depth z from pile center r can be shown in Equation (13).

$$\tau(z, r) = G_s \frac{dD_s}{dr} \quad (13)$$

According to the principle of pile–soil deformation coordination, the pile–soil interface shear force is equal, shear stress in the soil can be shown in Equation (14).

$$\tau(z, r) = \tau_p(z) \frac{r_1}{r} \quad (14)$$

Combining Equations (13) and (14), the soil displacement can be expressed in Equation (15).

$$dD_s = \frac{\tau_p(z, r)}{G_s} dr = \frac{\tau_p(z) r_1}{G_s} \frac{dr}{r} \quad (15)$$

According to Equation (15) can calculate the soil displacement outside of the pile–soil interface, which was shown in Equation (16).

$$D_s = \frac{\tau_p(z) r_1}{G_s} \int_{r_1}^{r_2} \frac{dr}{r} = \frac{\tau_p(z) r_1}{G_s} \ln\left(\frac{r_2}{r_1}\right) \quad (16)$$

where r_1 is the pile radius, m; r_2 is the disturbance radius, m (The reference radius is usually considered to be 20-fold r_1); G_s is the shear modulus of soil, Pa.

(1) Soil displacement calculation for TPPR

By substituting Equation (2) τ_{p1} equation into Equation (16), TPPR displacement D_{s1} can be solved, as shown in Equation (17).

$$D_{s1} = \int_0^{x_1} \frac{C + K_0[\gamma z + \sigma(z)] \tan \varphi r_1}{G_s} \ln\left(\frac{r_2}{r_1}\right) dz \quad (17)$$

(2) Soil displacement calculation for ER

By substituting Equation (2) τ_{p2} equation into Equation (16), TPPR displacement D_{s2} can be solved, as shown in Equation (18).

$$D_{s2} = \int_{x_1}^{x_3} \frac{\tau_{u2} \frac{z-\delta}{x_3-\delta} r_1}{G_s} \ln\left(\frac{r_2}{r_1}\right) dz \quad (18)$$

(3) Soil displacement calculation for ER

By substituting Equation (2) τ_{p3} equation into Equation (16), ER displacement D_{s3} can be solved, as shown in Equation (19).

$$D_{s3} = \int_{x_3}^{x_4} \frac{A \times [1 - \exp(-B \times \varepsilon)] r_1}{G_s} \ln\left(\frac{r_2}{r_1}\right) dz \quad (19)$$

Figure 4 presents a simplified flowchart that depicts the comprehensive methodology utilized in this study.

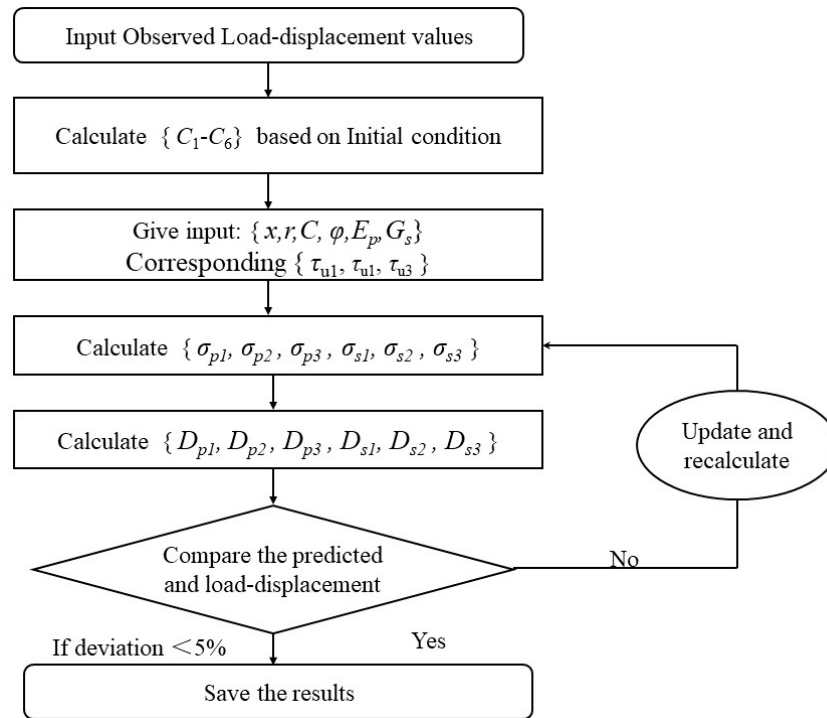


Figure 4. Flowchart of the methodology.

3. Model Application

In order to check the reliability of the calculates mode, based on the references [48] and the detailed properties of the soil strata for different loads are presented in Table 1. The specifications for the cast-in-situ bored pile, the concrete strength level of the foundation pile is C30, the elastic modulus of the pile body $E = 3.0 \times 10^4$ MPa, and the weighted average shear modulus of the soil on the side of the pile is $G_s = 3.18$ MPa, model prototype shown in Figure 5.

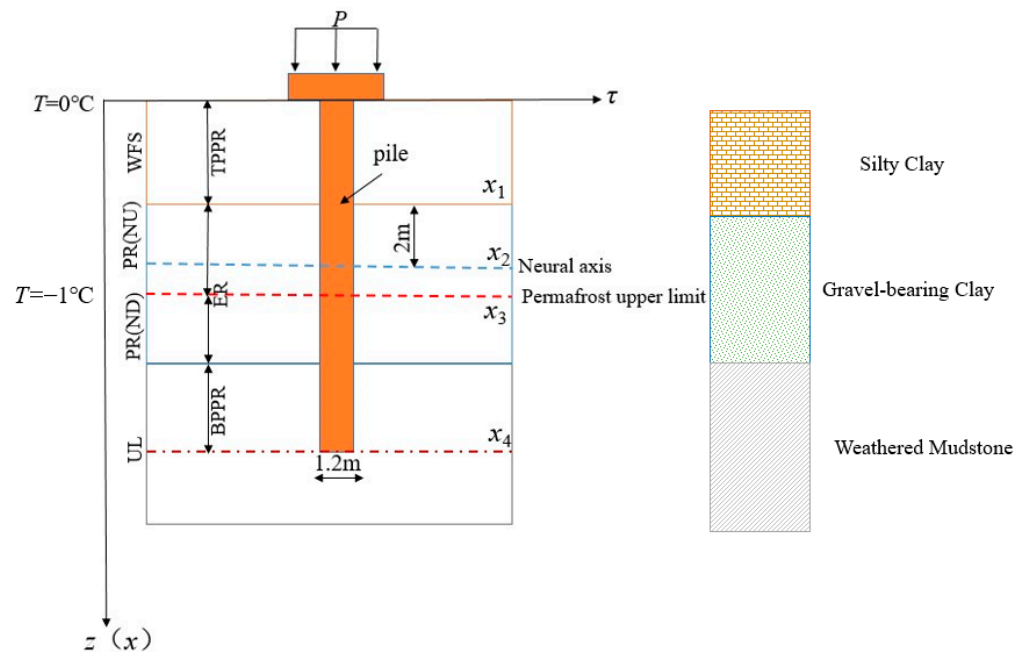


Figure 5. Vertical force diagram for pile and soil elements.

Table 1. Geotechnical characteristics of pile load.

Pile Length (m)	Pile Diameter (m)	Stratum Depth (m)	Stratum Description	Soil Type	Shear Parameters		γ (kN/m ³)
					C (kPa)	φ (°)	
20	1.0	0–2, [0– x_1]	WFS	Silty Clay	2	17	18.1
		2–6, [x_1 – x_2]	PR(NU)	Gravel-bearing Clay	22	28	18.6
		6–10, [x_2 – x_3]	PR(ND)		24	30	18.6
		10–20, [x_3 – x_4]	UL	Weathered Mudstone	20	40	22.0
18	0.8	0–1.5, [0– x_1]	WFS	Silty Clay	2	17	18.1
		1.5–5, [x_1 – x_2]	PR(NU)	Gravel-bearing Clay	22	28	18.6
		5–10, [x_2 – x_3]	PR(ND)		24	30	18.6
		10–18, [x_3 – x_4]	UL	Weathered Mudstone	20	40	22.0
16	0.6	0–1, [0– x_1]	WFS	Silty Clay	2	17	18.1
		1–4, [x_1 – x_2]	PR(NU)	Gravel-bearing Clay	22	28	18.6
		5–8, [x_2 – x_3]	PR(ND)		24	30	18.6
		8–16, [x_3 – x_4]	UL	Weathered Mudstone	20	40	22.0

C—effective cohesion, φ —effective friction angle, γ —unit weight of the soil.

3.1. Case Study 1

The different load-displacement for Case Study 1 is shown in Figure 6. The calculated results of this model are consistent with the *P-D* curve trend of Zhao's test results. With the increase of load, the pile displacement increases slowly in the range of 0–200 kN, and then the pile displacement increases quickly. According to the calculation of this model, when the pile length is 20 m, the diameter is 1.0 m, and the pile top bears the load of 0–1000 kN, the pile displacement range from 0 to 13.6 mm, while Zhao's test results show that the pile length is 20 m, diameter is 1.0 m, and the pile displacement range from 0 to 12.9 mm, which can conclude the calculate model results are more conservative than the test results.

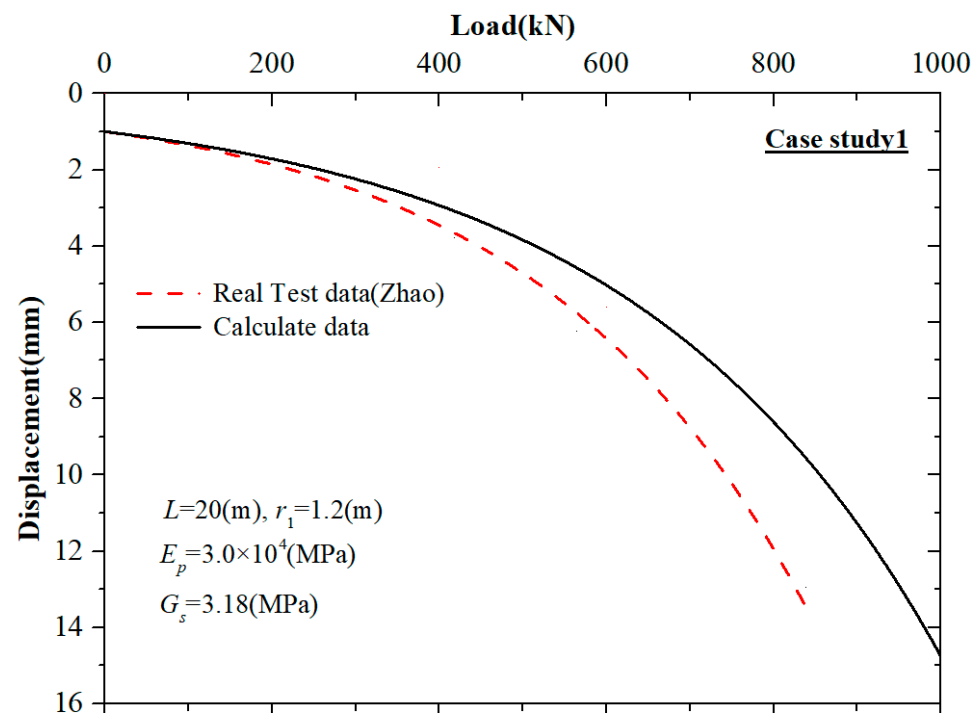


Figure 6. Comparison of measured and predicted load-displacement curves for Case study 1.

The Different load and displacement, along with pile depth curves for Case Study 1, are shown in Figure 7. With the increase of depth and temperature decreased, pile displacement firstly increases and then decreases, and the maximum value appears in PR(NU) and ER regions. When the pile length is 20 m, the diameter is 1.0 m, and the

maximum displacement pile body displacement is 13.6 mm. It can be seen that when the load is less than 400 kN, maximum displacement increases slowly with the increase in load, and its increase rate is relatively slow. When the load is greater than 400 kN, the maximum displacement of the pile increases rapidly. The displacement of piles increases rapidly in the WFS regions ($-1\text{ }^{\circ}\text{C} \leq T \leq 0\text{ }^{\circ}\text{C}$) under the action of the upper load, and gradually increases to the maximum displacement after entering the lying frozen soil area, and the maximum displacement occurs in the region above the upper limit of permafrost.

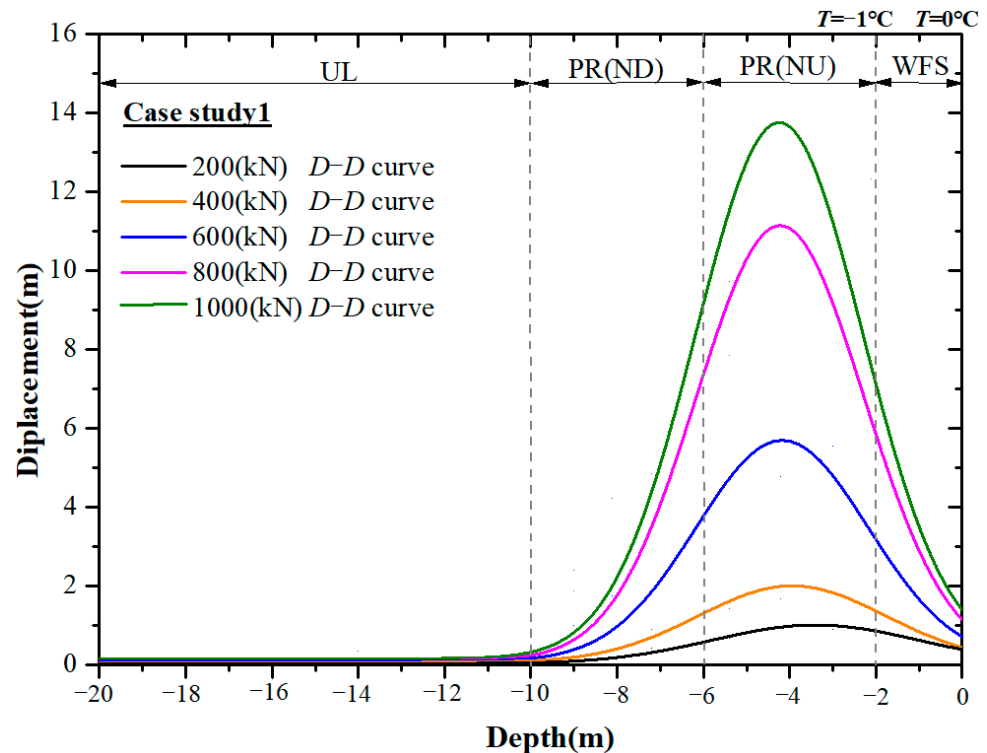


Figure 7. Different load and displacement along with pile depth curves for Case Study 1.

3.2. Case Study 2

Figure 8 presents a similar analysis, results, and comparison of measured and predicted P - D curves for same Zhao's test data. The length and diameter of the pile installed are 18 m and 0.8 m, respectively. According to the calculation model, when the pile top bears the load of 0–1000 kN, the pile displacement ranges from 0 to 20.43 mm, while Zhao's test results show that the pile length is 20 m, diameter is 1.0 m, and the pile displacement range from 0 to 12.9 mm. It can be concluded that when the pile diameter is larger, the pile length is longer, and the pile displacement is smaller. The predicted P - D curve trend using the calculated model closely matches what can be expected of the observed P - D curve.

The Different load and displacement, along with pile depth curves for Case Study 2, are shown in Figure 9. With the increase of depth, pile displacement first increases and then decreases, and the maximum value appears in PR(NU) in PR(NU) and ER regions. When the pile length is 18 m, the diameter is 0.8 m, and the maximum displacement pile body displacement is 20.43 mm. It can be seen that when the load is less than 400 kN, maximum displacement increases slowly with the increase in load, and its increase rate is relatively slow. When the load is greater than 400 kN, the maximum displacement of the pile increases rapidly. It can be proved that the displacement of piles increases rapidly in the WFS regions ($-1\text{ }^{\circ}\text{C} \leq T \leq 0\text{ }^{\circ}\text{C}$) under the action of the upper load, and gradually increases to the maximum displacement after entering the lying frozen soil area, and the maximum displacement occurs in the region above the upper limit of permafrost.

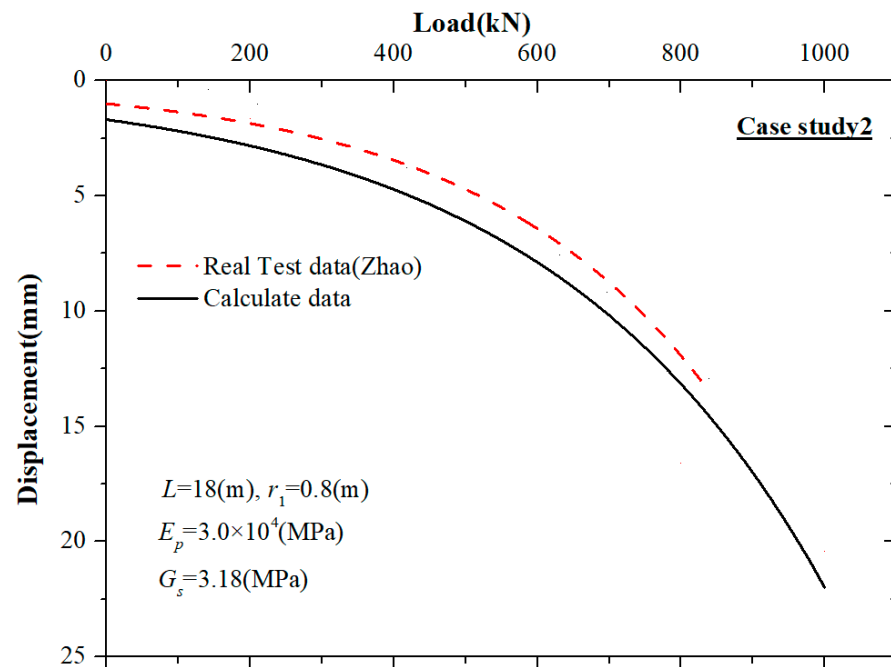


Figure 8. Comparison of measured and predicted load-displacement curves for Case Study 2.

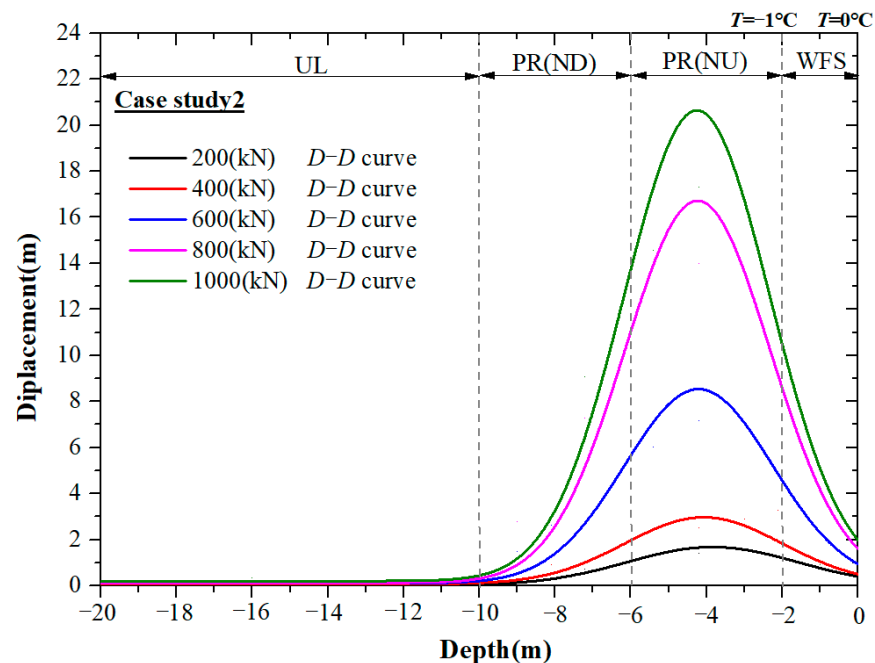


Figure 9. Different load and displacement along with pile depth curves for Case Study 2.

3.3. Case Study 3

Comparing observed and estimated P - D curves for a cyclic pile in different lengths and radii, Figure 10 shows findings similar to the above two case studies. The pile is 16 m long and has a diameter of 0.6 m. Based on the calculation model, when the pile top bears the load of 0–1000 kN, the pile displacement ranges from 0 to 27.26 mm, while Zhao's test results show that the pile length is 20 m, diameter is 1.0 m, and the pile displacement range from 0 to 12.9 mm. It can be concluded that when the pile diameter is larger and the pile length is longer, the pile displacement is smaller. The predicted P - D curve trend using the calculated model closely matches what can be expected for the observed P - D curve.

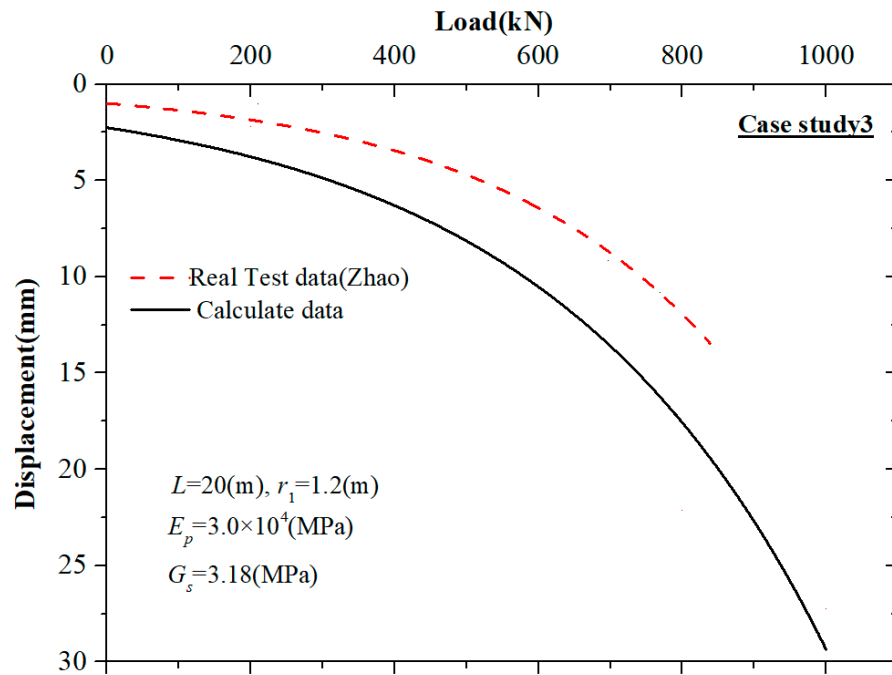


Figure 10. Comparison of measured and predicted load-displacement curves for Case Study 3.

Figure 11 presents a similar analysis, results, and comparison of measured and predicted curves for the same two case studies. With the increase of depth, pile displacement first increases and then decreases, and the maximum value appears in PR(NU) and ER regions. When the pile length is 16 m, the diameter is 0.6 m, and the maximum displacement pile body displacement is 27.26 mm. It can be seen that when the load is less than 400 kN, maximum displacement increases slowly with the increase in load, and its increase rate is relatively slow. When the load is greater than 400 kN, the maximum displacement of the pile increases rapidly.

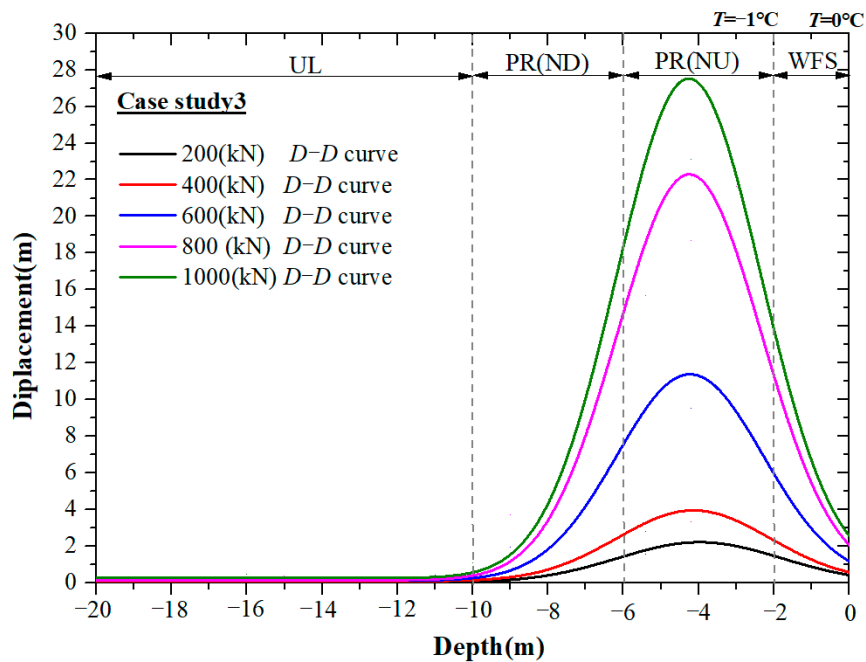


Figure 11. Different load and displacement along with pile depth curves for Case Study 3.

4. Discussions

External load imposed on pile foundations is transmitted to the surrounding warm frozen soil through different mechanisms, including contact surface friction. Figure 12 illustrates the different pile diameter-pile length-maximum displacement results for the calculated model in the same loading conditions, respectively. When the value of pile diameter and pile length is larger, the pile behaves as a friction end-bearing pile, and interaction coefficients for large diameter and long piles are bigger than the others. When the value of pile diameter and pile length is small because the interaction area decreases, the interaction coefficient becomes small. The stress and deformation of the soil on the pile side are big, so the shear deformation and interaction with adjacent soil are big.

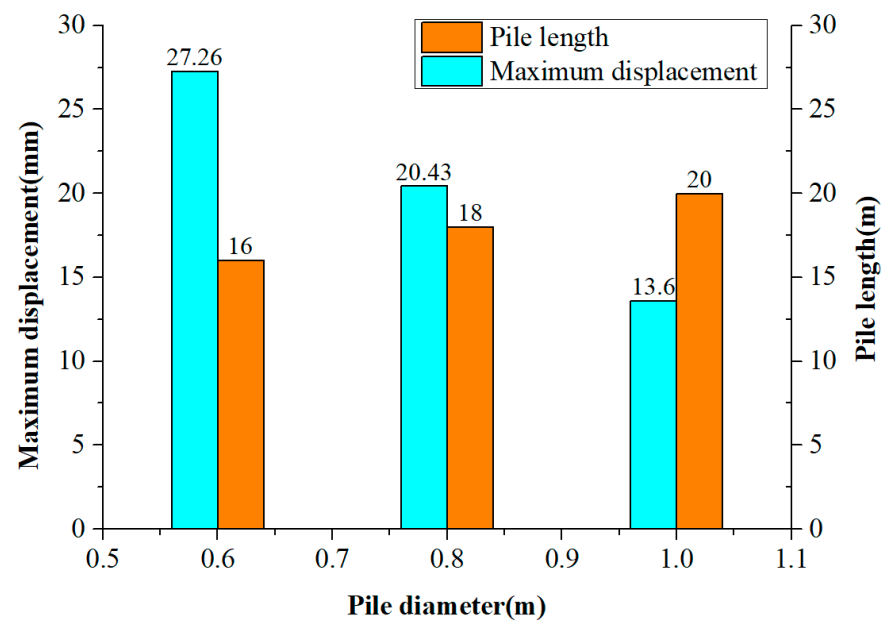


Figure 12. Comparison of different Pile diameters for Pile length and Maximum displacement.

5. Conclusions

Based on the shear displacement theory and load transfer method, WFS foundation pile–soil equilibrium equations for driving open-ended piles under different soil depth regions were developed, and the different regions' displacement of the WFS pile–soil system was derived. The equilibrium differential equations of soil elements inside the pile were established as well. The results of the proposed analytical solution were compared with existing research results to verify the reasonability. The main conclusions were summarized as follows:

- (1) A simple and novel calculated pile displacement model for WFS foundation in different regions was established; subsequently, the pile–soil equilibrium equations under WFS foundation conditions were developed.
- (2) Based on the calculation equation of the WFS pile–soil system, the displacement calculation equation of WFS soil during driving under a static load was derived. With the increase of depth, pile displacement first increases and then decreases, and the maximum value appears in PR(NU) in PR(NU) and ER regions.
- (3) The maximum displacement occurs regions for calculate models were investigated, and the reasonability of analytical solution was verified through comparing with existed research results.

Therefore, the proposed method was effective for the analysis of the WFS pile–soil system for piling projects. However, the results were relatively coarse because the parameters were assigned average values; if more accurate parameter values were used, the applicability of the results would be improved.

Author Contributions: Conceptualization, G.S.; Methodology, H.D.; Supervision, Z.W.; Investigation, L.G.; Software, L.L.; Writing—original draft, Y.H. All authors have read and agreed to the published version of the manuscript.

Funding: This research was supported by the National Natural Science Foundation of China (Grant Nos. 42301156 and 52308204), Natural Science Foundation of Shanxi Province (Grant Nos. 2023-JC-QN-0626 and 2024JC-YBMS-436) and Shaanxi Provincial Key Laboratory of Geotechnical and Underground Space Engineering open fund (Grant No. YT202302).

Data Availability Statement: The raw data supporting the conclusion of this article will be made available by the authors, without undue reservation.

Conflicts of Interest: Authors Lijun Gu and Hongzu Dang were employed by the company China State Construction Engineering Corporation Aecom Consultant Co., Ltd. The remaining authors declare that the research was conducted in the absence of any commercial or financial relationships that could be construed as a potential conflict of interest.

References

1. Sun, G.C.; Yao, G.; Zhang, J.M.; Li, B.; Li, J.-Q.; Lian, W.-P.; Wei, Y. Stabilized effects of L-S cement-mixed batter pile composite foundation for existed warm frozen soil subgrade. *J. Mt. Sci.* **2023**, *20*, 542–556. [[CrossRef](#)]
2. Sun, G.C.; Zhang, J.M.; Dang, Y.S.; Ding, C. Microstructure and strength features of warm and ice-rich frozen soil treated with high-performance cements. *J. Mt. Sci.* **2019**, *16*, 1470–1482. [[CrossRef](#)]
3. Zhang, H. The deformation prediction method of expansive soil foundation by shrinkage test. *Rock Soil Mech.* **1999**, *20*, 22.
4. Anbazhagan, P.; Bajaj, K. Region-specific correlations between VVS30 and time-averaged VS and SPT-N values at different depths for the indo-Gangetic basin. *Indian Geotech. J.* **2020**, *50*, 454–472. [[CrossRef](#)]
5. Guo, L.; Yu, Q.H.; Yin, N.; You, Y.; Wang, J.; Sun, Y.; Chen, K. Analysis of Expansive Two-phase closed thermosyphon-induced frost jacking of piles and foundation instability in a thawed permafrost area. *Nat. Hazard.* **2024**, *120*, 619–637. [[CrossRef](#)]
6. Liu, J.K.; Wang, T.F.; Tai, B.W.; Lv, P. A method for frost jacking prediction of single pile in permafrost. *Acta Geotech.* **2020**, *15*, 455–470. [[CrossRef](#)]
7. Ashutosh, K.; Sonu, K. Settlement Based Load-Bearing in a Combined Pile–Raft Foundation. *Geotech. Geol. Eng.* **2024**, *42*, 1405–1421. [[CrossRef](#)]
8. Xu, Y.; Niu, X. The implementation of a Random Forest model utilizing meta-heuristic algorithms to forecast the undrained shear strength. *Multiscale Multidiscip. Model. Exp. Des.* **2023**, *15*, 455–470. [[CrossRef](#)]
9. Kondner, R. Hyperbolic stress–strain response: Cohesive soils. Discussion. *J. Soil Mech. Found. Div. ASCE* **1963**, *89*, 241–242. [[CrossRef](#)]
10. Anjana, B.R. Study of the Effect of Pile Type for Supporting Basal Reinforced Embankments Constructed on Soft Clay Soil. *J. Mt. Sci.* **2013**, *20*, 542–556.
11. Semenova, N.P.; Malyshev, A.V.; Timoveev, A.M.; Bolshev, K.N.; Stepanov, A.A. Mathematical Model of the Temperature Control at the Base of a Building with a Slab Foundation on a Compacted Seasonally Thawing Layer. *Soil Mech. Found. Eng.* **2023**, *60*, 391–398. [[CrossRef](#)]
12. Abzhaimov, R.S. Hypothesis concerning distribution of normal forces of frost heaving across the lower surface of solidly frozen soil layers beneath foundations. *Soil Mech. Found. Eng.* **2004**, *41*, 27–33. [[CrossRef](#)]
13. Zhao, X.Y.; Mao, X.S.; Wu, Q.; Huang, W.; Wang, Y. Study on Shear Characteristics of Interface between Frozen Soil and Pile during Thawing Process in Permafrost Area. *Adv. Civ. Eng.* **2022**, *2022*, 1755538. [[CrossRef](#)]
14. Li, L.; Deng, Y.S. Strengthening mechanism of plum blossom pile composite foundation. *Acta Geotech.* **2023**, *21*, 875–886. [[CrossRef](#)]
15. Wang, H.L.; Zhang, J.M.; Wei, S.C.; Sun, Z.; Zhang, H. Experimental and numerical interpretation on composite foundation consisting of soil-cement column within warm and ice-rich frozen soil. *J. Mt. Sci.* **2023**, *21*, 313–321. [[CrossRef](#)]
16. Tang, L.; Yang, L.; Wang, X.; Yang, G.; Ren, X.; Li, Z.; Li, G. Numerical analysis of frost heave and thawing settlement of the pile–soil system in degraded permafrost region. *Environ. Earth Sci.* **2021**, *80*, 693–712. [[CrossRef](#)]
17. Li, Q.; Zhang, Y.; Chen, C.; Wen, M.; Guan, W.; Duan, W. Dynamic response of a large-diameter end-bearing pile in permafrost. *Sci. Rep.* **2024**, *14*, 582–598. [[CrossRef](#)]
18. Abdulghader, A.; Mohammad, R. A Quick Approach for Estimating Load Transfer of Conventional and Helical Piles in Ice-Rich Frozen Soils. *Geotech. Geol. Eng.* **2021**, *39*, 2927–2944. [[CrossRef](#)]
19. Kumar, S.; Kumar, A. Effect of infiltration on single-pile and monopile-raft foundation embedded in unsaturated sand. *Int. J. Geomech.* **2023**, *23*, 04022288. [[CrossRef](#)]
20. Huang, Y.; Zhuang, X.; Wang, P.; Zong, Z. Axial Behavior of Pressure Grouted Helical Piles Installed in Marine Soft Clay Based on Full-Scale Field Tests. *Geotech. Geol. Eng.* **2022**, *40*, 5799–5812. [[CrossRef](#)]
21. Lv, Y.; Zhang, D.; Li, P.; Zheng, C. A Theoretical Analysis of the Vertical Shearing Mechanism of the H-Pile. *Soil Mech. Found. Eng.* **2015**, *52*, 122–130. [[CrossRef](#)]

22. Yoo, W.K.Y.; Kim, B.-I.I.; Cho, W.J. Model Test Study on the Behavior of Geotextile-Encased Sand Pile in Soft Clay Ground. *KSCE J. Civ. Eng.* **2015**, *19*, 592–601. [[CrossRef](#)]
23. Wang, Z.; Xie, X.; Wang, J. A new nonlinear method for vertical settlement prediction of a single pile and pile groups in layered soils. *Comput. Geotech.* **2012**, *45*, 118–126. [[CrossRef](#)]
24. Aoki, N.; Velloso, D.D.A. An approximate method to estimate the bearing capacity of piles. In Proceedings of the 5th Pan-American Conference of Soil Mechanics and Foundation Engineering, Buenos Aires, Argentina, 17–22 November 1975; Volume 1, pp. 367–376. Available online: <https://www.researchgate.net/publication/291797985> (accessed on 1 March 2017).
25. Poulos, H.G.; Davis, A.J. Foundation design for the emirates twin towers, Dubai. *Can. Geotech. J.* **2005**, *42*, 716–730. [[CrossRef](#)]
26. Yang, L.-G.; Ji, W.-D.; Zhang, Y.-T.; Ren, Q.-W.; Shen, R.-T. Analysis of Expansive Earth Pressure of Pile Foundation under Repeated Immersion. *Int. J. Civ. Eng.* **2023**, *21*, 875–886. [[CrossRef](#)]
27. Lin, C.; Liu, Q.; Su, Y.; Yue, C.; Zeng, L. Load transfer of the disconnected pile. *Acta Geotech.* **2024**, *39*, 2927–2944. [[CrossRef](#)]
28. Zhuang, X.R.; Zhao, H. Numerical analyses of pile performance in laterally spreading frozen ground crust overlying liquefiable soils. *Earthq. Eng. Eng. Vib.* **2018**, *17*, 491–499. [[CrossRef](#)]
29. Rajashree, S.S.; Sitharam, T.G. Nonlinear finite element modeling of batter piles under lateral load. *J. Geotech. Geoenvironmental Eng. ASCE* **2001**, *127*, 604–612. [[CrossRef](#)]
30. Wang, J.; Jia, K.; Rafique, R.; Guo, L.; Yu, Q.; Yue, Y.; Yuan, C. Changes of backfill soil of tower foundation in the permafrost regions with warm ice-rich frozen soil on the Qinghai–Tibet Plateau. *Environ. Earth Sci.* **2016**, *75*, 1416–1426. [[CrossRef](#)]
31. Mahdy, M. On the Impact of Soil Density on Soil Reaction and Structural Responses. *Arab. J. Sci. Eng.* **2022**, *47*, 4347–4361. [[CrossRef](#)]
32. Xu, J.J.; Xu, X.; Yao, W.J. New calculation method for the settlement of long-short-pile composite foundation based on virtual soil-pile model. *Arab. J. Geosci.* **2022**, *15*, 870–886. [[CrossRef](#)]
33. Armaleh, S.; Desai, C.S. Load-deformation response of axi-ally loaded piles. *J. Geotech. Eng.* **1987**, *113*, 1483–1500. [[CrossRef](#)]
34. Yan, M.; Guo, S.; Zhang, H.; Song, X.; Xiao, H. Investigation on Load Transfer in Geosynthetic-Reinforced Pile-Supported Embankments. *Indian Geotech. J.* **2024**, *39*, 2927–2944. [[CrossRef](#)]
35. Bohn, C.; Lopes dos Santos, A.; Frank, R. Development of axial pile load transfer curves based on instrumented load tests. *J. Geotech. Geoenvironmental Eng.* **2017**, *143*, 04016081. [[CrossRef](#)]
36. Hirayama, H. Load-settlement analysis for bored piles using hyperbolic transfer functions. *Soils Found.* **1990**, *30*, 55–64. [[CrossRef](#)]
37. Liu, J.; Xiao, H.B.; Tang, J.; Li, Q.S. Analysis of load-transfer of single pile in layered soil. *Comput. Geotech.* **2004**, *31*, 127–135. [[CrossRef](#)]
38. Zhang, Q.Q.; Zhang, Z.M.; He, J.Y. A simplified approach for settlement analysis of single pile and pile groups considering interaction between identical piles in multilayered soils. *Comput. Geotech.* **2010**, *37*, 969–976. [[CrossRef](#)]
39. Bazaraa, A.R.; Kurkur, M.M. N-values used to predict settlements of piles in Egypt. In *Use of In Situ Tests in Geotechnical Engineering*; ASCE: Reston, VA, USA, 1986; pp. 462–474.
40. Han, F.; Salgado, R.; Prezzi, M.; Lim, J. Shaft and base resistance of non-displacement piles in sand. *Comput. Geotech.* **2017**, *83*, 184–197. [[CrossRef](#)]
41. Zhang, L.J.; Wu, X.; Zhang, Y.G.; Xie, Y. Analysis of swelling characteristics of the original expansive soils without loads. *Hydrogeol. Eng. Geol.* **2015**, *42*, 96–100. [[CrossRef](#)]
42. Wang, Z.; Yang, J.X.; Kuang, J.J.; An, J.Y.; Luo, Y.D. Application of filter paper method in field measurement of matric suction. *J. Geotech. Eng.* **2003**, *25*, 405–408.
43. Fleming WGK A new method for single pile settlement prediction and analysis. *Geotechnique* **1992**, *42*, 411–425. [[CrossRef](#)]
44. Horikoshi, K.; Randolph, M.F. On the definition of raft—Soil stiffness ratio for rectangular rafts. *Géotechnique* **1997**, *47*, 1055–1061. [[CrossRef](#)]
45. Azzam, W.R.; Basha, A.M. Utilization of micro-piles for improving the sub-grade under the existing strip foundation: Experimental and numerical study. *Innov. Infrastruct. Solut.* **2018**, *3*, 44. [[CrossRef](#)]
46. Sakr, M.A.; Nazir, A.K.; Azzam, W.R.; Sallam, W.F. Behavior of grouted single screw piles under inclined tensile loads in sand. Innovative Infrastructure Solutions. *Electron. J. Geotech. Eng. EJGE* **2016**, *2*, 571–591. Available online: <https://www.researchgate.net/publication/2921312070> (accessed on 1 March 2017).
47. Dey, A.; Basudhar, P.K. Bearing capacity of surface footings on reinforced sandy bed: A revised regression model. *Indian Geo-Tech. J.* **2022**, *52*, 448–462. [[CrossRef](#)]
48. Zhao, Y.; Mao, X.; El Naggar, M.H.; Li, W. Characteristics of Resilient Modulus of Weathered Phyllite Subgrade during Saturation Process. *J. Transp. Eng. Part B Pavements* **2022**, *148*, 04022027. [[CrossRef](#)]

Disclaimer/Publisher’s Note: The statements, opinions and data contained in all publications are solely those of the individual author(s) and contributor(s) and not of MDPI and/or the editor(s). MDPI and/or the editor(s) disclaim responsibility for any injury to people or property resulting from any ideas, methods, instructions or products referred to in the content.